Polyoxometalate/carbon black modified glassy carbon electrode for the detection of dopamine

Xiong Liu
Wuhan Institute of Technology
Cailing Zhong
Wuhan Institute of Technology
Jun Ji
Wuhan Institute of Technology
Wei Yang
Wuhan Institute of Technology
Zhengfang Tian
Yichang Chen
Wuhan Institute of Technology
Qifeng Tian (qftian@wit.edu.cn)
Wuhan Institute of Technology

Research Article

Keywords: sensor, differential pulse voltammetry, carbon black, dopamine, phosphotungstic acid

Posted Date: January 3rd, 2023

DOI: https://doi.org/10.21203/rs.3.rs-2416065/v1

Abstract

Dopamine (DA) is a crucial neurotransmitter in the central nervous system (CNS) of human and multicellular animal brains. In this paper, we report for the first time the synthesis of C/PWA composites by doping phosphotungstic acid (PWA) on carbon black nanoparticles by impregnation method. The synthesized materials were characterized and corroborated using high-resolution scanning electron microscopy, X-ray diffraction spectroscopy (XRD) and Fourier transform infrared spectroscopy. The synthesized C/PWA composite modified glassy carbon (GC) electrodes were used as selective electrocatalysts for dopamine (DA) oxidation process. The electrochemical redox behavior of DA was studied with cyclic voltammetry (CV). Under optimized conditions, DA was detected by differential pulse voltammetry (DPV) and the calibration plot showed linearity (R^2 = 0.9988) over the range of DA concentrations of 10 μM-600 μM with a detection line of 0.1 μM. The sensor's capability to detect DA in commercial DA injections in real time has been successfully demonstrated.

1 Introduction

The central nervous system (CNS) of human and multicellular animal brains contains an endogenous nitrogenous organic molecule called dopamine (DA), which is essential as a neurotransmitter[1], and likewise in the physiological regulatory functions of the human metabolic, cardiovascular, renal and hormonal systems DA also acts as a local chemical messenger in mammals [2]. Abnormal levels of DA in the human body may cause a variety of diseases, such as schizophrenia, Alzheimer's disease, Parkinson's disease[3] and attention deficit hyperactivity disorder[4], which seriously endanger human physical and mental health. Therefore, accurate and simple determination of the amount of DA is important for the prevention and diagnosis of diseases. Current methods for the detection of DA include high performance liquid chromatography[5], fluorescence[6], spectrophotometry[7], and electrochemical methods[3, 8–16]. Compared with traditional detection methods, electrochemical methods are characterized by low cost, easy translocation detection, block response time and high sensitivity. It has been widely used for the detection of drugs and certain biological components. The unmodified glassy carbon electrode has poor selectivity, so the electrode needs to be modified to improve its selectivity for better DA detection. To address these issues, chemically modified electrodes have been widely used for selective detection of DA, including carbon nanomaterials, ionic liquids, redox-active enzymes, molecular imprinted polymers[17], and organometallic compounds[18, 19]. Vulcan XC-72 conductive carbon black is a good carrier material with good electrical conductivity, large specific surface area, high availability and low cost. Usually the carbon material is functionalized and modified with modifiers to obtain better conductivity and selectivity. The modifiers are nanoparticles[20–27], cyclodextrins[28], and polymetallic oxides[29–31]. Phosphotungstic acid (PWA), which has catalytic properties, is a polymetallic oxygenate with high proton transfer capacity[32] and has properties such as good stability, long lifetime in solution, easy separation and non-corrosiveness. PWA can participate in the catalytic process when it is present on the modified electrode[33, 34].

2 Experimental

2.1 Apparatus

The Shanghai Chenhua electrochemical workstation was used to conduct the electrochemical experiments. A three-electrode system was used, including of a saturated calomel electrode reference electrode, a platinum rode auxiliary electrode, and a glassy carbon electrode (GCE) with a diameter of 3mm as the working electrode. A JEOL-7800F scanning electron microscope (SEM) was used to characterize the morphology of the material. The material was analyzed using a D8 Advance X-ray diffractometer (XRD) from Bruker, Germany, with Cu Kα radiation (λ = 1.5418 nm Å) and a scan range of 2θ from 10 to 90°. With KBr spheres, infrared spectra between 400 and 4000 cm^{-1} were collected using an Alpha Centaurt FT-IR spectrometer.

2.2 Chemicals

Dopamine was purchased from Wuhan Geochem Co. Ltd. The other chemical reagents (analytically pure) used in the experiments were purchased from China National Pharmaceutical Group Chemical Reagent Co. Ltd. The solutions used in the experimental procedure were prepared with ultrapure water. Glassy carbon electrodes are used after polishing. The dopamine solution was configured to a certain concentration with ultrapure water before starting the electrochemical test.

2.3 Preparation of phosphotungstic acid/carbon black composite

The carbon black was first impregnated with nitric acid and stirred overnight, then filtered and washed with ultrapure water, then dried at 80 ℃ for 6 hours under vacuum and crushed. Take 100 mg of treated carbon black and add it to a single mouth flask, take 50 ml of phosphotungstic acid solution with a concentration of 6×10^{-4} M and add it to the flask, stir it overnight under the environment of 80 ℃ water bath, then filter it while it is hot, wash it with 1L of water and dry it for 4 hours at 60 ℃ under vacuum, that is, C/PWA powder.

2.4 Pretreatment and modification of GCE

The glassy carbon electrode (3 mm in diameter) was polished with 0.3μm and 0.05μm α-Al_2O_3 in turn, and the surface was cleaned with anhydrous ethanol and ultrapure water in an ultrasonic environment in turn, and then dried naturally after cleaning and set aside. Weigh 3 mg of the prepared C/PWA powder into 0.5 mL of 5% mass fraction of Nafion solution and obtain a uniform dispersion by ultrasonic dispersion. Take 5 μL of the dispersion and put it on the clean GCE surface, and allow it to naturally dry at ambient temperature to produce the improved C/PWA electrode.

3 Results And Discussion

3.1 Characterization of materials

The SEM images of C and C/PWA samples are exhibited in Fig. 1. It can be seen from Fig. 1a that C presents the microstructure of nanoparticle clusters. Figure 1b shows the microstructure of C/PWA at the same magnification. It can be found that the C nanoparticles modified by PWA are relatively enlarged. The full binding of PWA to C nanoparticles can exert the advantage of synergistic effects. The specific surface area of the modified C material is increased, which helps to improve the conductivity of the C nanoparticles.

Figure 2 shows the XRD results of C nanoparticles and C/PWA samples. Figure 2 shows the XRD pattern of C with a cluster-like granular microstructure. The XRD pattern of C is revealed to be consistent with the one of typical C. The XRD pattern of C/PWA nanoparticles shown in Fig. 2 shows several distinct diffraction peaks characteristic of PWA (No. JCPDS 50–0655) which indicates that PWA is present in the modifier layer.

The IR spectra of C, PWA, and C/PWA are displayed in Fig. 3. Tensile vibration maxima in the C spectra can be found at 1560 cm^{-1} (C = C) and 3500 cm^{-1} (O-H). Peak vibrations in the PWA spectrum can be seen at 1088 cm^{-1} (P-Oa), 900 cm^{-1} (W-Ob-W), and 810 cm^{-1} (W-Oc-W) (While Ob and Oc are the oxygens of the W-Ob-W bridge, which connects two distinct yet identical W_3O_{13} groups, respectively, Oa stands for the center tetrahedral PO_4 oxygen). These characteristic peaks can also be observed in C/PWA which indicates the presence of $PW_{12}O_{40}^{3-}$ anions in the composite structure and confirms the successful doping of PWA.

3.2 Electrochemical profile of dopamine at modified electrodes

The responses of the same concentration of DA on three different modified electrodes, GCE, C/GCE, and C/PWA/GCE, are shown in Fig. 4. The voltammogram measured by cyclic voltammetry(CV) shows the redox situation of DA at the modified electrode. As can be seen from the figure, after the modification of GCE, it can be found that the redox current response situation is significantly increased, and GCE has enhanced its conductivity by the modification of activated carbon, while after the modification of GCE by C/PWA, the current response situation is greatly increased, indicating that the synergistic effect of C and PWA makes the electron transfer efficiency increase. Figure 5 shows the differential pulse voltammetry (DPV) of DA on GCE, C/GCE, and C/PWA/GCE. In the case of bare GCE, there was almost no current response, and a significant current response appeared through the modification of GCE by activated carbon. Last but not least, C/PWA causes a noticeable rise in peak current, showing that the electrocatalytic function of PWA makes GCE treated with C and PWA more likely to experience oxidation.

3.3 Analysis of surface area and impedance

The electrochemical behavior of the electrodes in 5.0 mM $K_3[Fe(CN)_6]/K_4[Fe(CN)_6]$ and 0.1 M KCl solutions was investigated using the electrochemical impedance spectroscopy (EIS) technique. The

Nyquist curve obtained is shown in Fig. 6. Among the three different electrodes, the charge transfer resistance of the GCE modified with C/PWA was lower than that of the C/GCE, and bare GCE electrode which were C/PWA/GCE (81.4 Ω), C/GCE (179.2 Ω), and bare GCE (371.5 Ω). This result is probably due to the increased effective surface area of the electrode and the special electrocatalytic properties of PWA, which increase the electron transfer rate[35]. Based on the aforementioned findings, it can be concluded that C/PWA/GCE exhibits more effective interfacial electron transport than bare GCE and C/GCE. The modification of the GCE electrode can be confirmed by comparing the electron transfer effect of the modified electrode with that of the bare electrode. Therefore, by obtaining cyclic voltammograms at different scan rates in $K_3Fe(CN)_6$, the Randles-Sevcik equations[9, 36] for the effective surface areas of GCE, C/GCE and C/PWA/GCE were calculated as follows:

$$I_P = (2.69 \times 10^5)\, n^{3/2}\, A\, D^{1/2}\, v^{1/2}\, C$$

*I*p is the peak anode current (A), n is the number of transferred electrons (n = 2), *A* is the effective surface area of the electrode in cm^2, *D* is the diffusion coefficient of $K_3Fe(CN)_6$ (5×10^{-6} cm^2 s^{-1}), *v* is the scan rate (V/s), and *C* is the concentration of $K_3Fe(CN)_6$ (mol/cm^3). The slope of a plot of *I*p versus $v^{1/2}$ is then used to calculate *A*. The calculated effective surface area values for bare GCE, C/GCE and C/PWA/GCE were 0.0554 cm^2, 0.0638 cm^2 and 0.1939 cm^2, respectively. It is evident that C/PWA/GCE has a much higher effective surface than bare GCE by a factor of 3.5, demonstrating the superiority of its electrochemical activity.

3.4 Conditions optimization

3.4.1 pH effect

In phosphate buffer, the effects of pH on the oxidation peak current values of DA (100 M) were investigated. The results are presented in Fig. 7. Figures 7a and 7c show that the peak current increases starting at pH 6 and climbs until it reaches a maximum at pH 7.5. The next experiment used phosphate buffer solution to bring the solution's pH to 7.5. Furthermore, when the pH of the buffer solution was varied from 6 to 8, With rising pH, the maximal oxidation potential of DA moved toward being lower, indicating the involvement of protons in these oxidation processes. The linear relationship between Ep and pH is shown in Fig. 7b, and the linear equation is Ep = -0.0648pH + 0.5832 (R^2 = 0.998), with the absolute value of the slope approximately equal to the theoretical value of 0.059 VpH^{-1}, demonstrating that at the C/PWA/GCE modified electrode, the amount of electrons and protons transported during the redox process of DA is equivalent, which is consistent with the literature[16]. Figure 8 depicts the potential electrochemical oxidation of DA at the C/PWA/GCE modified electrode.

3.4.2 Effect of C/PWA content

By altering the C/PWA content, the impact of the modifier content on the DA oxidation peak current was examined. Different masses of C/PWA (1, 2, 3, 4 and 5 mg) were dispersed in a specific volume of Nafion solution to test the impact of mass. Figure 9 illustrates the peak currents attained by the modified electrode as a result of the dispersed modifier's drop coating approach of modifying the bare GCE. The data showed that as the dispersion mass grew from 1 to 5 mg, the oxidation peak current of DA initially increased and subsequently declined. The peak current is increased because of the increase in C/PWA content and the gradual increase in the number of electrons transferred. The later peak current decreases because of the increase in C/PWA content and the thicker coating due to the drop coating method of modifying the electrode, which has a hindering effect on electron transfer, and therefore the peak current response is reduced. Therefore, 3 mg was chosen as the optimum dispersion mass in C/PWA.

3.4.3 Effect of the modification time

The C/PWA enrichment time was investigated under the conditions of optimal C/PWA dispersion mass, and the results of the investigation are shown in Fig. 10. From the analysis of the graph, it is known that when the enrichment time increases from 3 min to 7 min, the peak current reaches a higher level at 4 min, so 4 min is chosen as the best enrichment time.

3.5 Electrochemical analysis of the modified electrodes

3.5.1 Analysis of scan rate

The effect of the scan rate on the peak current and peak potential of C/PWA/GCE in the presence of DA concentration of 100 μM was tested using cyclic voltammetry under the above optimal test conditions. The CV for different scan rates (20-400mVs^{-1}) were tested as shown in Fig. 11a. As the scan rate increases from 20mVs^{-1} to 400mVs^{-1}, the peak anode and cathode currents of the DA also increase. It was shown that the peak current increases linearly with the square root of the sweep speed ($^{1/2}$) (Fig. 11b). The linear regression equations are Ipa (μA) = 17.88 $^{1/2}$-89.05 and Ipc (μA) = -16.54 $^{1/2}$+94.36 with a 0.996 correlation coefficient, which indicates that the electron transfer process is diffusion controlled[13].

3.5.2 Chronoamperometric studies

The diffusion coefficient (*D*) of DA in the electrochemical process was determined using chronoamperometric measurements. In a phosphate buffer solution containing a specific concentration of DA, a constant voltage of 1 V was supplied to the modified working electrode, and its current was measured as a function of time. Since the mass transfer process in the solution is completely controlled by diffusion, the generated I-t curve displays changes in the gradient of concentration close to the electrode surface. This situation entails the diffusion layer gradually expanding as the electroactive species are gradually removed. Consequently, the Cottrel equation can be used to express the current's

strength as follows:

$$I = \frac{nFACD^{1/2}}{\pi^{1/2}t^{1/2}} = Kt^{-1/2}$$

I is the current (A), *C* is the volume concentration (mol cm^{-3}), *A* is the electrode surface area (cm^2), *t* is the time (s), and *D* is the diffusion coefficient (cm^2 s^{-1}). *I* equals the current (A), *C* equals the volume concentration (mol cm^{-3}), *A* equals the electrode surface area (cm^2), *t* equals the time (s), and *D* equals the diffusion coefficient (cm^2 s^{-1}). Figure 12 shows the timing current plots of C/PWA/GCE for three different concentrations of DA (50, 100 and 150 µM) at potential steps of 1 V. The related *I* vs. $t^{-1/2}$ plots are displayed in inset a. The slope of these plots was used to extract the diffusion coefficients. For this purpose, the slope of the resulting line is depicted as a function of DA concentration (inset b). According to the resulted slope, the *D* of DA is calculated to be equal to 7.57×10^{-7} cm^2 s^{-1}.

3.6 Analytical performances

By measuring DA under ideal experimental conditions using C/PWA/GCE in phosphate buffer solution and the DPV method, the calibration curve for the modified sensor was created. Figure 13 shows the voltammograms obtained for the different concentrations. According to the calibration curve (inset Fig. 13), the current is linear with concentration from 10×10^{-6} to 600×10^{-6} M ($R^2 = 0.9988$) and the linear equation is Ip (µA) = 0.42059C (µM) + 196.315. The detection limit (S/N = 3) for 5 replicate measurements of the blank solution is 0.1×10^{-6}M.

3.7 Reproducibility and repeatability

The C/PWA/GCE sensor's repeatability measurements for five consecutive measurements are shown in Fig. 14a. The associated peak current measurements display an RSD value of 0.56%, which indicates that the sensor has good repeatability. The reproducibility measurements of the C/PWA/GCE sensor are given in Fig. 14b. Five different C/PWA/GCE sensors were manufactured by the same fabrication method and the same test method was used to obtain the peak currents under the same conditions. These several DA sensors' peak current responses exhibit good agreement and minimal fluctuation. These peak current measurements had an RSD value of 1.1%, demonstrating the C/PWA/GCE sensors' strong repeatability.

3.8 Interference effects

The effect of ions that may have the ability to interfere during DA measurements, which are usually components of pharmaceutical or biological media, was examined. Interference effects were examined by measuring 100 µM DA solutions containing various concentrations of foreign substances under optimal conditions. The data obtained showed no significant effect of Na^+, Ca^{2+}, Mg^{2+}, K^+, Cl^-, NO^{3-}, PO_4^{3-}, CO_3^{2-} ions (500-fold concentration) as well as uric acid, ascorbic acid and glucose. The results showed a good selectivity of C/PWA/GCE.

3.9 Analytical applications

To evaluate the practicality of the proposed sensor, the concentration of DA in dopamine hydrochloride injection was determined by this sensor. The purchased dopamine hydrochloride injection (10 mg/ml) from Shanghai He Feng Pharmaceutical Co., Ltd. was diluted to a certain concentration and assessed under the optimal experimental conditions with the addition of 50 μM and the detection amount of 51.2 ± 1.8 μM with the recoveries of 98.8%-105% and the relative standard deviations less than 5%. This indicates that C/PWA/GCE has good prospects for use in the detection of DA.

3.10 Comparison of the sensors in this study with those in the literature

The linear range, detection limit, and sensitivity of the developed electrochemical sensor (as three important analytical factors) and previously reported linear range, detection limit, and sensitivity for measuring DA are shown in Table 1. The given data demonstrate that the constructed sensor is superior to other sensors in determining the detection range of DA. The better properties of this sensor can be attributed to the combination of the excellent electrocatalytic properties of polyoxometalates and the electrochemical modification properties of activated carbon, which have higher sensitivity than other modifiers in the modified electrodes.

Table 1
Comparison of different modified sensors for DA detection.

Electrode/modifier	Linear range (μM)	Detection limit (μM)	Ref.
GR/GCE	4.0-100.0	2.64	[9]
^{1}PdNPs/CNF/CPE	0.5–160	0.2	[37]
gold nanosheets/GCE	2-298	0.28	[16]
Pd@Fe3O4/GCE	0.96–107	0.41	[11]
MWCNTs/GCE	3-200	0.8	[8]
C/PWA/GCE	10–600	0.1	This work

4 Conclusions

Electrochemical sensors were fabricated by carbon black nanoparticles doped with glassy carbon electrodes modified with phosphotungstic acid. The successful formation of C/PWA composites was confirmed by SEM, XRD and FT-IR spectroscopy. Compared with the bare GCE electrode, C/PWA/GCE has a larger surface area and better conductivity, thus showing a better electrochemical capability of C/PWA/GCE. The sensor has a wide detection range and good selectivity in the detection of DA, and the existence of good reproducibility and repeatability of the sensor has been confirmed by repeated testing.

The detection limit of the sensor can reach 0.1×10^{-6} M. Thus, it can be seen that the C/PWA composite has a certain prospect of application in electrochemical sensing.

Declarations

Acknowledgements

This work was supported by the Natural Science Foundation of Hubei Province (Grant No. 2016CFA079) and the financial supports from the Opening Research Fund of Hubei Key Laboratory for Processing and Application of Catalytic Materials.

References

1. Montague PR, Hyman SE, Cohen JD (2004) Computational roles for dopamine in behavioural control. Nature 431:760–767
2. Heien MLAV, Khan AS, Ariansen JL, Cheer JF, Phillips PEM, Wassum KM, Wightman RM (2005) Real-time measurement of dopamine fluctuations after cocaine in the brain of behaving rats. PNAS 102:10023–10028
3. Soltani N, Tavakkoli N, Shahdost-Fard F, Salavati H, Abdoli F (2019) A carbon paste electrode modified with Al_2O_3-supported palladium nanoparticles for simultaneous voltammetric determination of melatonin, dopamine, and acetaminophen. Microchim Acta 186:540–553
4. Mallesha M, Manjunatha R, Nethravathi C, Suresh GS, Rajamathi M, Melo JS, Venkatesha TV (2011) Functionalized-graphene modified graphite electrode for the selective determination of dopamine in presence of uric acid and ascorbic acid. Bioelectrochemistry 81:104–108
5. Ye N, Gao T, Li J (2014) Hollow fiber-supported graphene oxide molecularly imprinted polymers for the determination of dopamine using HPLC-PDA. Anal Methods 6:7518–7524
6. Amjadi M, Manzoori JL, Hallaj T, Sorouraddin MH (2014) Strong enhancement of the chemiluminescence of the cerium(IV)-thiosulfate reaction by carbon dots, and its application to the sensitive determination of dopamine. Electrochim Acta 181:671–677
7. Khajehsharifi H, Pourbasheer E, Tavallali H, Sarvi S, Sadeghi M (2017) The comparison of partial least squares and principal component regression in simultaneous spectrophotometric determination of ascorbic acid, dopamine and uric acid in real samples. Arab J Chem 10:S3451–S3458
8. Alothman ZA, Bukhari N, Wabaidur SM, Haider S (2010) Simultaneous electrochemical determination of dopamine and acetaminophen using multiwall carbon nanotubes modified glassy carbon electrode. Sens Actuators B Chem 146:314–320
9. Kim YR, Bong S, Kang YJ, Yang Y, Mahajan RK, Kim JS, Kim H (2010) Electrochemical detection of dopamine in the presence of ascorbic acid using graphene modified electrodes. Biosens Bioelectron 25:2366–2369

10. Liu M, Chen Q, Lai C, Zhang Y, Deng J, Li H, Yao S (2013) A double signal amplification platform for ultrasensitive and simultaneous detection of ascorbic acid, dopamine, uric acid and acetaminophen based on a nanocomposite of ferrocene thiolate stabilized Fe(3)O(4)@Au nanoparticles with graphene sheet. Biosens Bioelectron 48:75–81
11. Liu Y, Zhu W, Wu D, Wei Q (2015) Electrochemical determination of dopamine in the presence of uric acid using palladium-loaded mesoporous Fe_3O_4 nanoparticles. Measurement 60:1–5
12. Palanisamy S, Velusamy V, Ramaraj S, Chen SW, Yang TCK, Balu S, Banks CE (2019) Facile synthesis of cellulose microfibers supported palladium nanospindles on graphene oxide for selective detection of dopamine in pharmaceutical and biological samples. Mater Sci Eng C 98:256–265
13. Reddaiah K, Reddy TM, Mallikarjuna K, Narasimha G (2013) Electrochemical detection of dopamine at poly(solochrome cyanine)/Pd nanoparticles doped modified carbon paste electrode and simultaneous resolution in the presence of ascorbic acid and uric acid: a voltammetric method. Anal Methods 5:5627–5636
14. Tootoonchi A, Davarani SSH, Sedghi R, Shaabani A, Moazami HR (2018) A Non-Enzymatic Biosensor Based on Pd Decorated Reduced Graphene Oxide Poly (2-anilinoethanol) Nanocomposite and Its Application for the Determination of Dopamine. J Electrochem Soc 165:B150–B159
15. Zhang K, Zhang N, Zhang L, Wang H, Shi H, Liu Q (2018) Simultaneous voltammetric detection of dopamine, ascorbic acid and uric acid using a poly(2-(N-morpholine)ethane sulfonic acid)/RGO modified electrode. RSC Adv 8:5280–5285
16. Zhang Q, Feng J, Wang A, Wei J, Lv Z, Feng J (2014) A glassy carbon electrode modified with porous gold nanosheets for simultaneous determination of dopamine and acetaminophen. Microchimica Acta 182:589–595
17. Shrivastava S, Jadon N, Jain R (2016) Next generation polymer nanocomposites based electrochemical sensors and biosensors: A review. Trac-trend Anal Chem 82:55–67
18. Jackowska K, Krysinski P (2012) New trends in the electrochemical sensing of dopamine. Anal Bioanal Chem 405:3753–3771
19. Sajid M, Nazal MK, Mansha M, Alsharaa A, Jillani SMS, Basheer C (2016) Chemically modified electrodes for electrochemical detection of dopamine in presence of uric acid and ascorbic acid: A review. Trac-trend Anal Chem 76:15–29
20. Liang C, Qiu H, Han Y, Gu H, Song P, Wang L, Kong J, Cao D, Gu J (2019) Superior electromagnetic interference shielding 3D graphene nanoplatelets/reduced graphene oxide foam/epoxy nanocomposites with high thermal conductivity. J Mater Chem C 7:2725–2733
21. Meng H, Zhang X, Pu Y, Chen X, Feng J, Han D, Wang A (2019) One-pot solvothermal synthesis of reduced graphene oxide-supported uniform PtCo nanocrystals for efficient and robust electrocatalysis. J Colloid Interface Sci 543:17–24
22. Niu H, Zhang L, Feng J, Zhang Q, Huang H, Wang A (2019) Graphene-encapsulated cobalt nanoparticles embedded in porous nitrogen-doped graphitic carbon nanosheets as efficient electrocatalysts for oxygen reduction reaction. J Colloid Interface Sci 552:744–751

23. Pang J, Mendes RG, Bachmatiuk A, Zhao L, Ta HQ, Gemming T, Liu H, Liu Z, Rummeli MH (2019) Applications of 2D MXenes in energy conversion and storage systems. RSC Adv 48:72–133
24. Rao CNR, Pramoda K (2019) Borocarbonitrides, BxCyNz, 2D Nanocomposites with Novel Properties. Bull Chem Soc Jpn 92:441–468
25. Sengottaiyan C, Jayavel R, Shrestha RG, Subramani T, Maji S, Kim JH, Hill JP, Ariga K, Shrestha LK (2019) Indium Oxide/Carbon Nanotube/Reduced Graphene Oxide Ternary Nanocomposite with Enhanced Electrochemical Supercapacitance. Bull Chem Soc Jpn 92:521–528
26. Shi Y, Feng J, Lin X, Zhang L, Yuan J, Zhang Q, Wang A (2019) One-step hydrothermal synthesis of three-dimensional nitrogen-doped reduced graphene oxide hydrogels anchored PtPd alloyed nanoparticles for ethylene glycol oxidation and hydrogen evolution reactions. Electrochim Acta 293:504–513
27. Thu NTA, Duc HV, Phong NH, Cuong ND, Hoan NTV, Khieu DQ (2018) Electrochemical Determination of Paracetamol Using Fe_3O_4/Reduced Graphene-Oxide-Based Electrode. J Nanomater 2018:1–15
28. Tandel RD, Seetharamappa J (2018) Porous Reduced Graphene Oxide β-cyclodextrin Modified Electrode as Enhanced Sensing Platform for the Determination of Dihydrochalcone: Phloretin. J Electrochem Soc 165:H629–H637
29. Rezvani MA, Aghbolagh ZS, Monfared HH, Khandan S (2017) Mono Mn(II)-Substituted Phosphotungstate@Modified Graphene Oxide as a High-Performance Nanocatalyst for Oxidative Demercaptanization of Gasoline. J Ind Eng Chem 52:42–50
30. Fernandes DM, Freir C (2015) Carbon Nanomaterial–Phosphomolybdate Composites for Oxidative Electrocatalysis. ChemElectroChem 2:269–279
31. Xu M, Liu C, Wang Y, Wang J, Feng J, Sha J (2021) A New Well–Dawson Polyoxometalate Based Compound Containing Helix for Electrochemical Uric Acid Biosensor. J Cluster Sci 31:1543–1552
32. Mosa J, Larramona G, Durán A, Aparicio M (2008) Synthesis and characterization of P_2O_5–ZrO_2–SiO_2 membranes doped with tungstophosphoric acid (PWA) for applications in PEMFC. J Membr Sci 307:21–27
33. Ammam M (2013) Polyoxometalates: formation, structures, principal properties, main deposition methods and application in sensing. J Mater Chem A 1:1–58
34. Gan T, Hu C, Chen Z, Hu S (2010) Fabrication and application of a novel plant hormone sensor for the determination of methyl jasmonate based on self-assembling of phosphotungstic acid–graphene oxide nanohybrid on graphite electrode. Sens Actuators B Chem 151:8–14
35. Chen Y, Yuan P, Wang A, Luo X, Xue Y, Zhang L, Feng J (2019) A novel electrochemical immunosensor for highly sensitive detection of prostate-specific antigen using 3D open-structured PtCu nanoframes for signal amplification. Biosens Bioelectron 126:187–192
36. Rezvani SA, Soleymanpour A (2019) Application of a sensitive electrochemical sensor modified with WO3 nanoparticles for the trace determination of theophylline. Microchem J 149:104005–104012

37. Huang J, Liu Y, Hou H, You T (2008) Simultaneous electrochemical determination of dopamine, uric acid and ascorbic acid using palladium nanoparticle-loaded carbon nanofibers modified electrode. Biosens Bioelectron 24:632–637

Figures

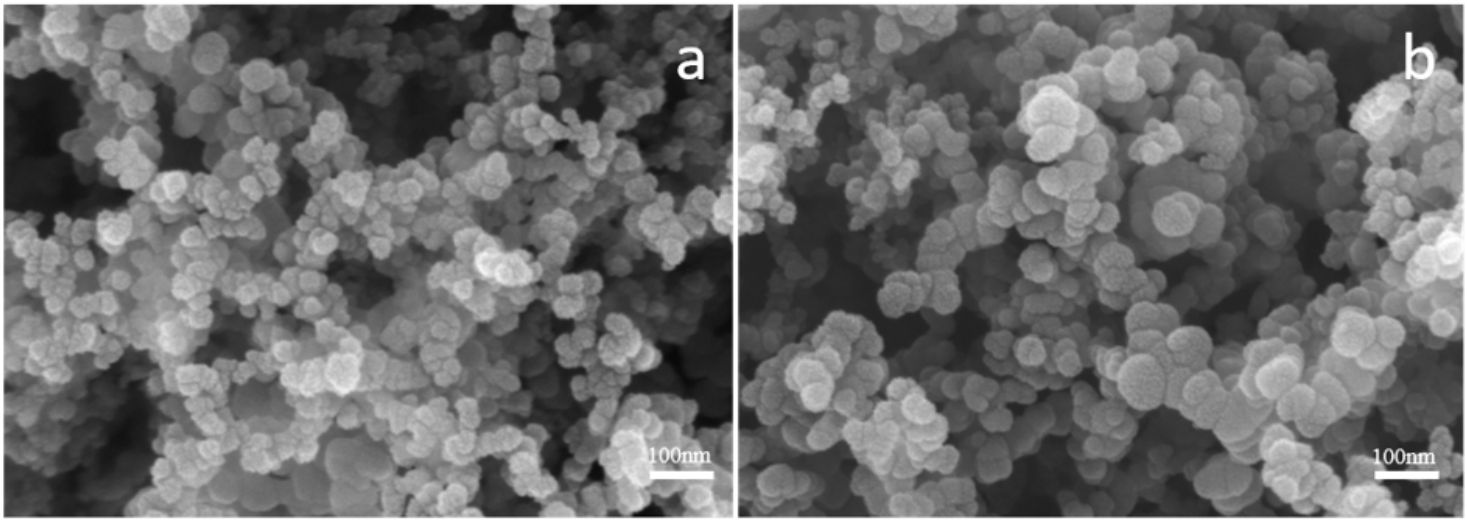

Figure 1

SEM images of (a) C nanoparticles and (b) C/PWA composites.

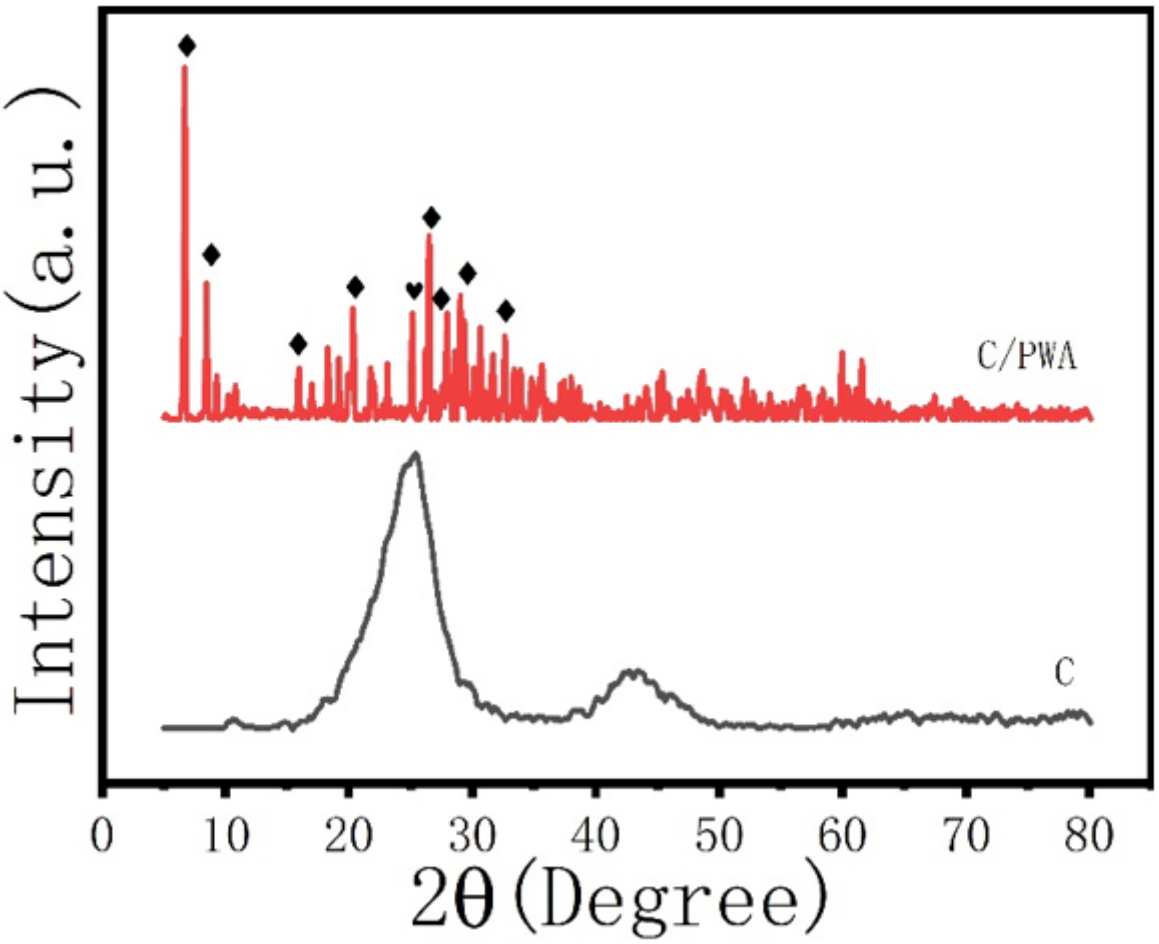

Figure 2

XRD analysis of C and C/PWA modifier layers (marked peaks are PWA peaks according to their standard patterns)

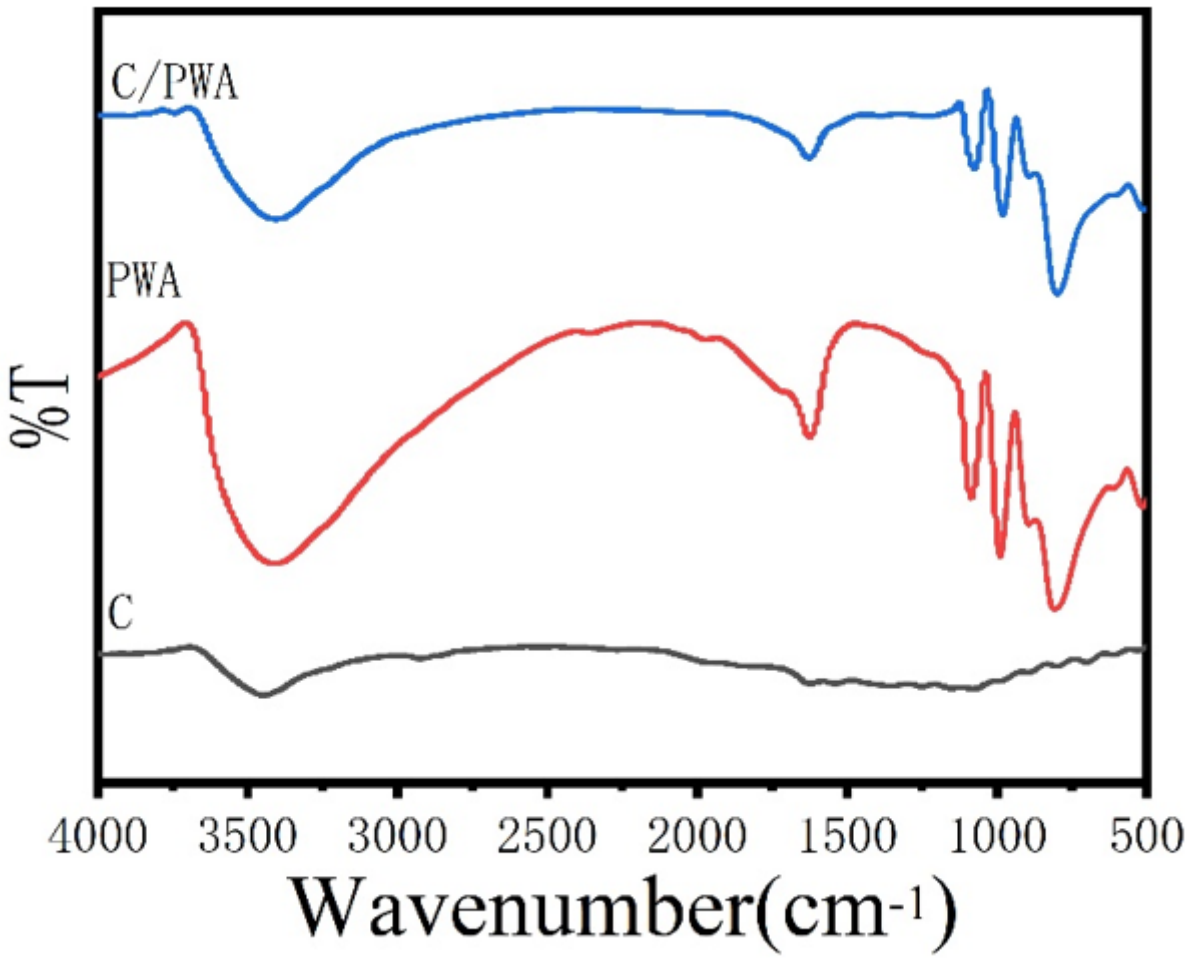

Figure 3

FT-IR spectrum of C, PWA, and C/PWA

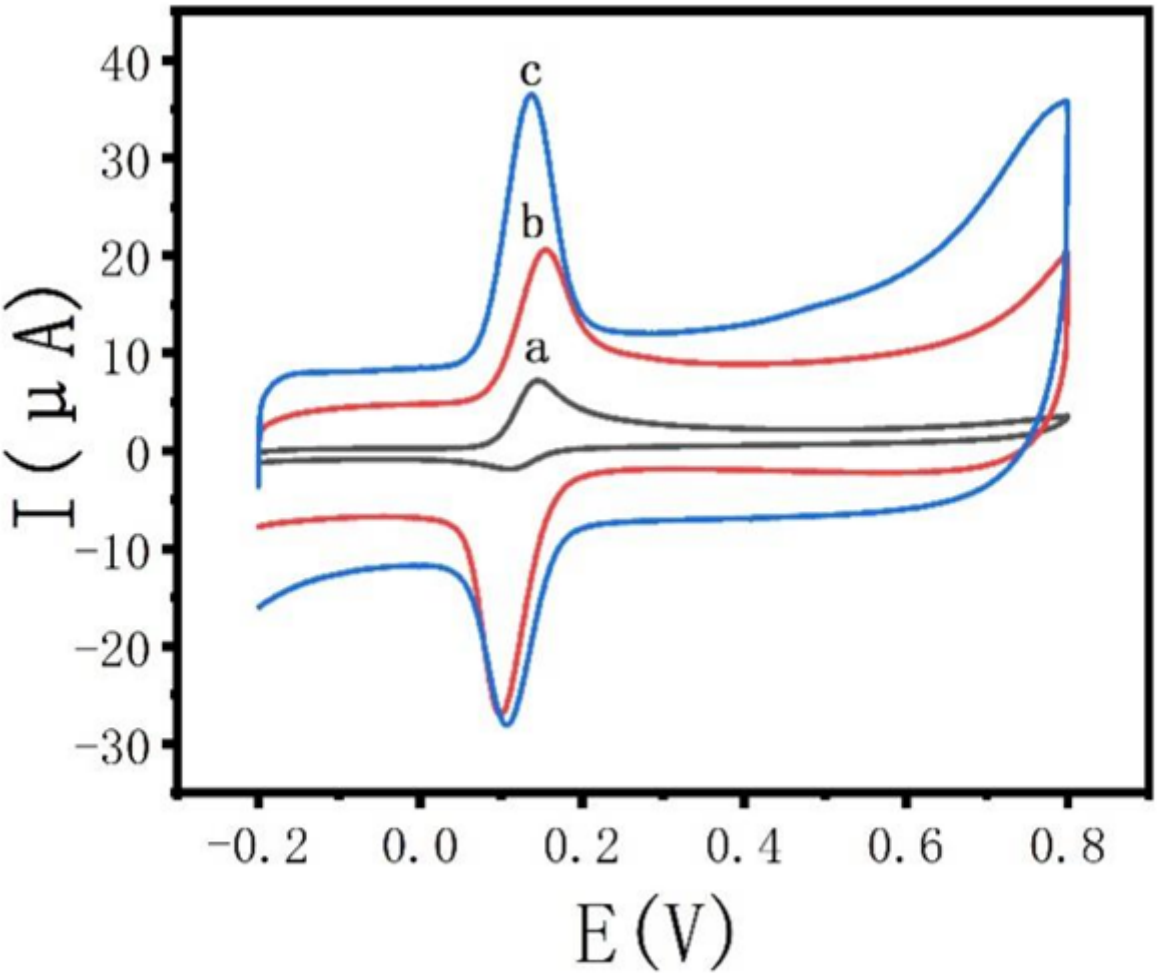

Figure 4

CV curves of 10 μM DA at the (a)bare GCE, (b)C/GCE and (c)C/PWA/GCE sensors.

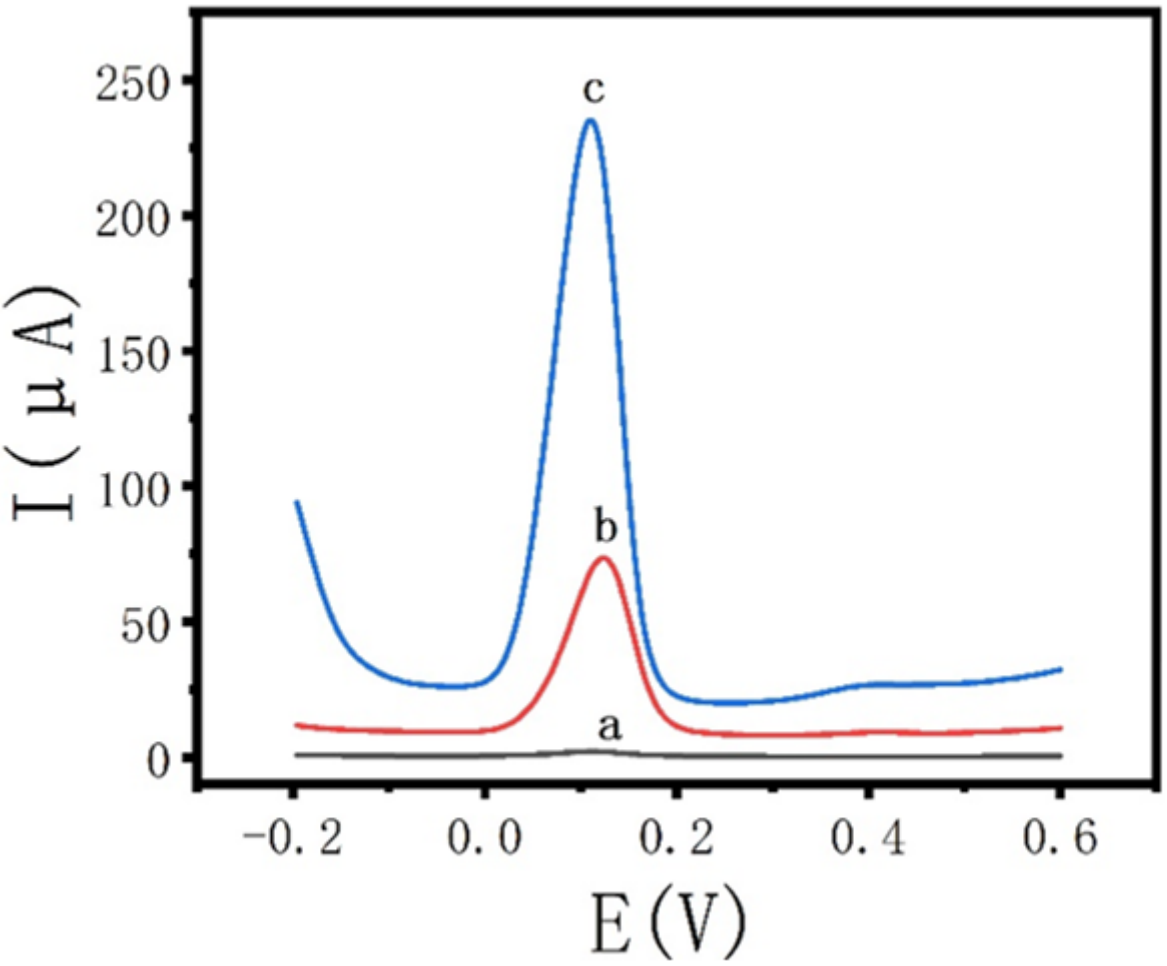

Figure 5

DPV plots of 100mM DA at the (a)bare GCE, (b)C/GCE and (c)C/PWA/GCE sensors.

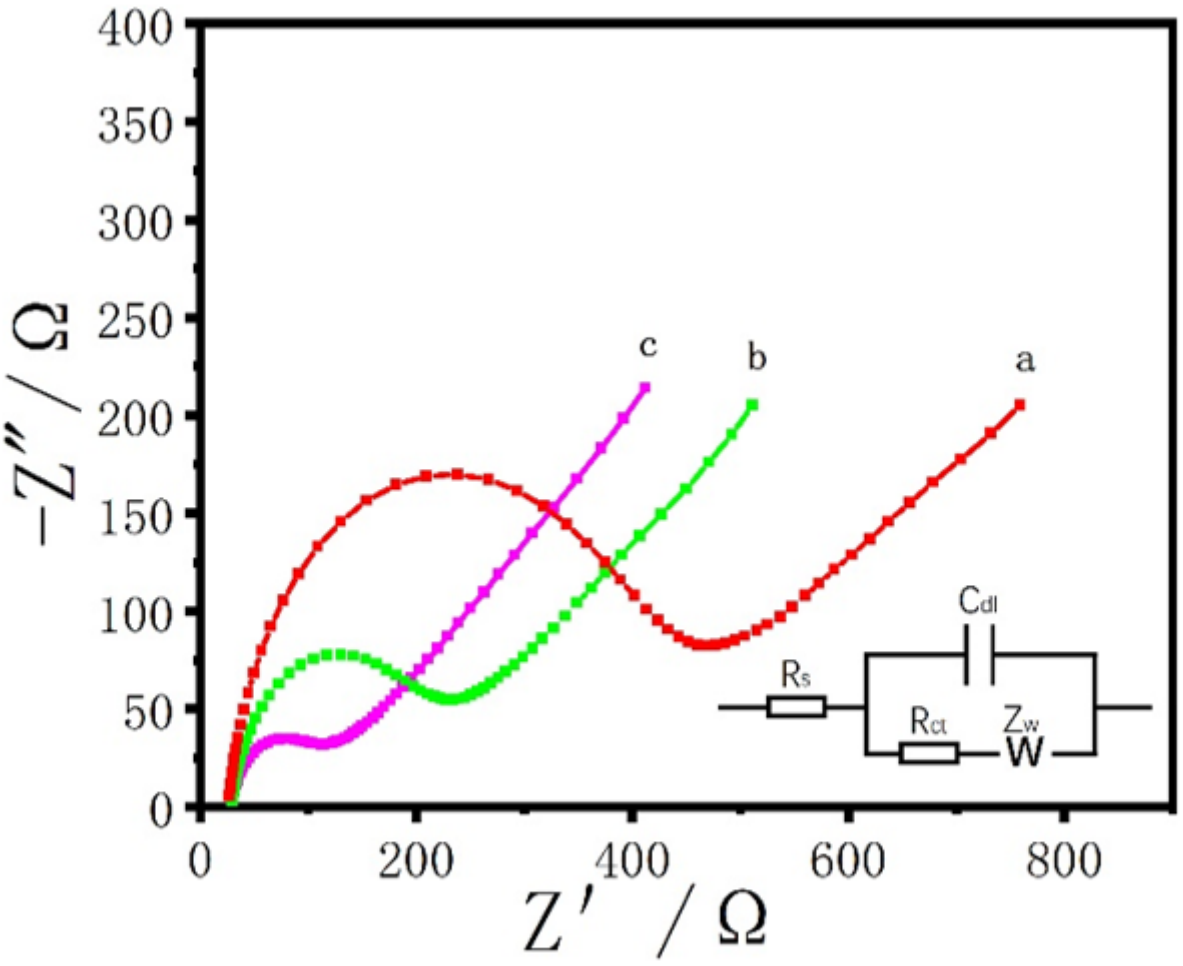

Figure 6

Nyquist curves of (a) GCE, (b) C/GCE and (c) C/PWA/GCE in 5 mM $[Fe(CN)_6]^{3-}$/$[Fe(CN)_6]^{4-}$ and 0.1 M KCl solutions.

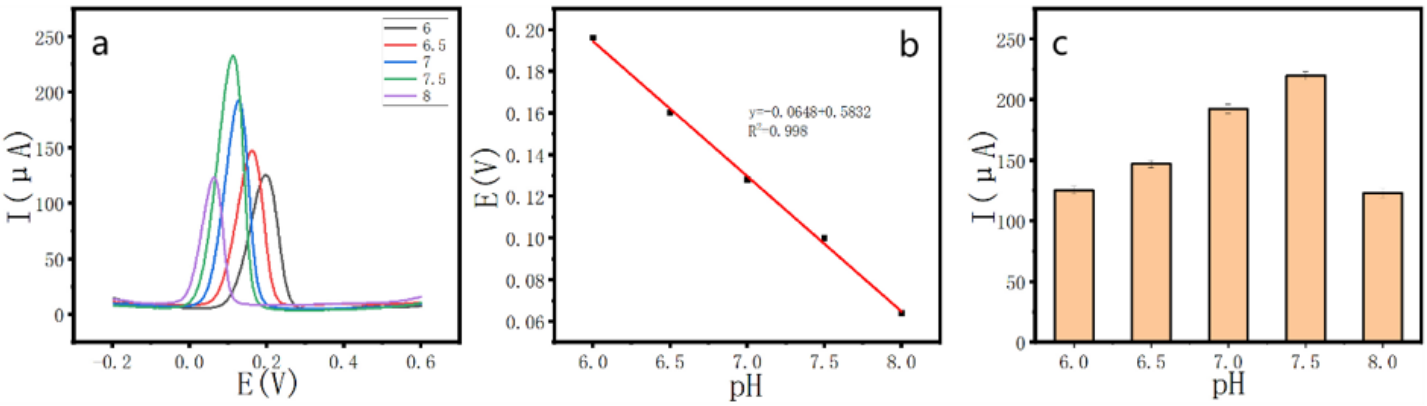

Figure 7

(a) Effect of pH value on DA detection performance on C/PWA/GCE sensor, (b) fitting relationship of pH value to peak potential, and (c) relationship between pH value and peak current.

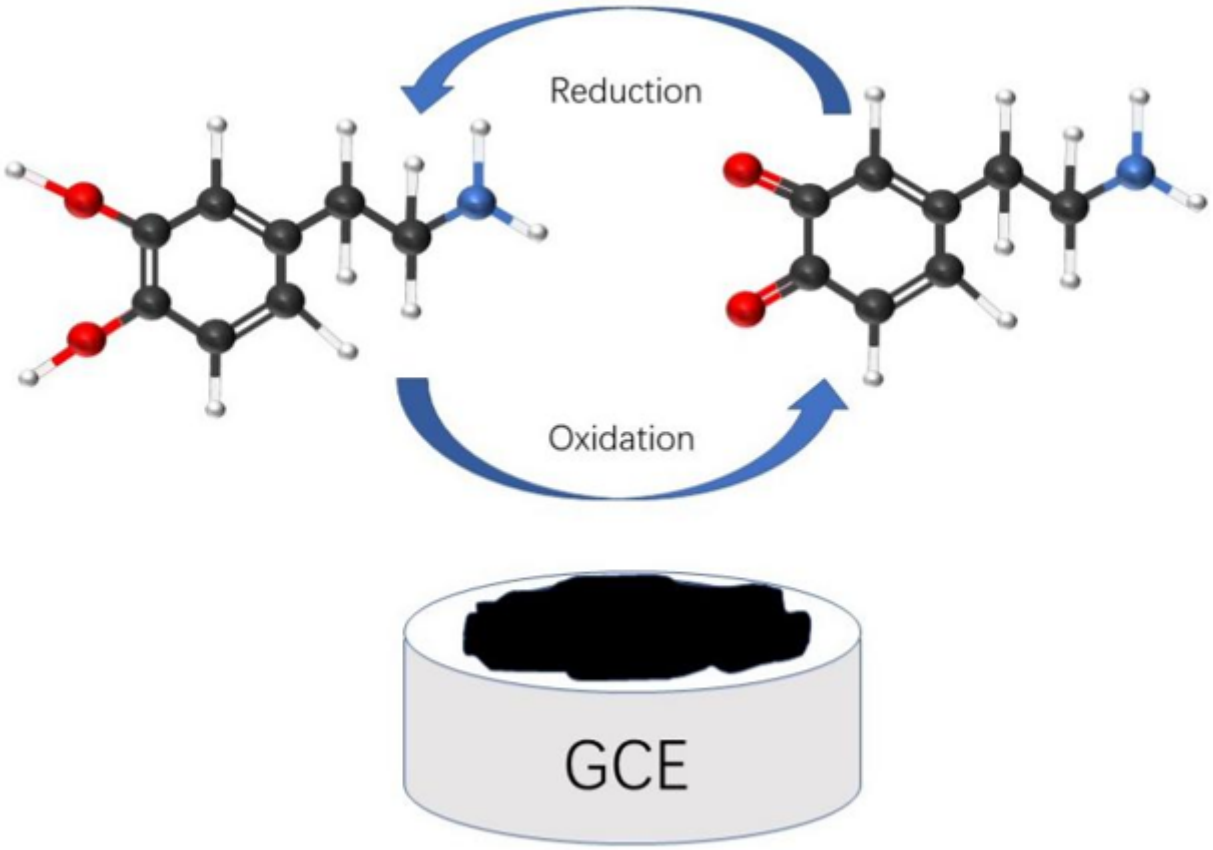

Figure 8

Proton/electron transfer mechanism of DA.

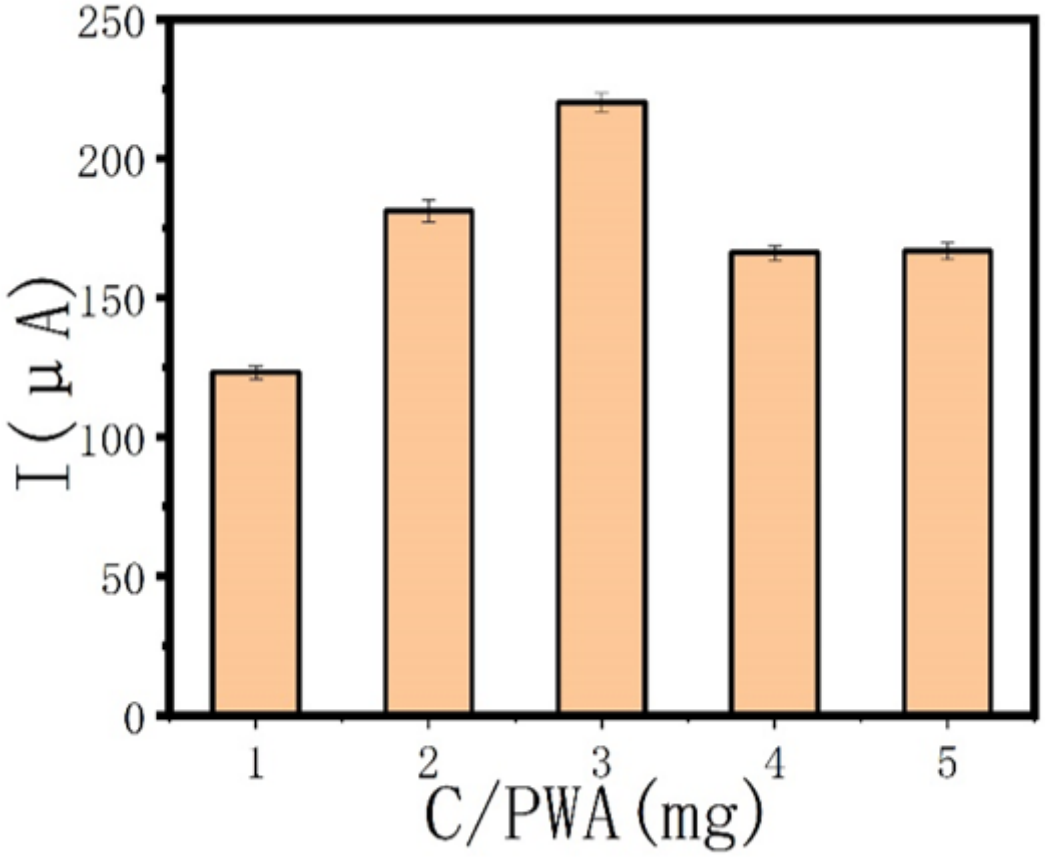

Figure 9

Effect of different C/PWA masses on the oxidation peak current of DA (100 μM).

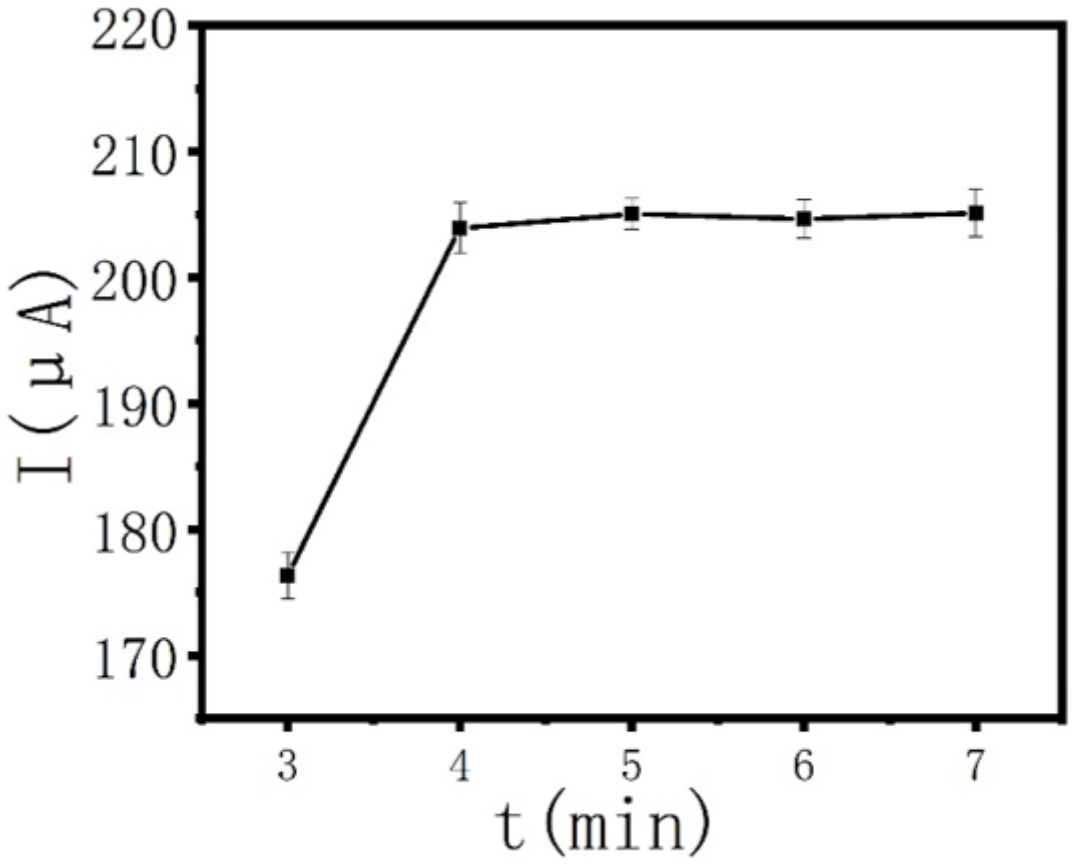

Figure 10

Effect of enrichment time on the oxidation peak current of DA (100 μM) at pH 7.5.

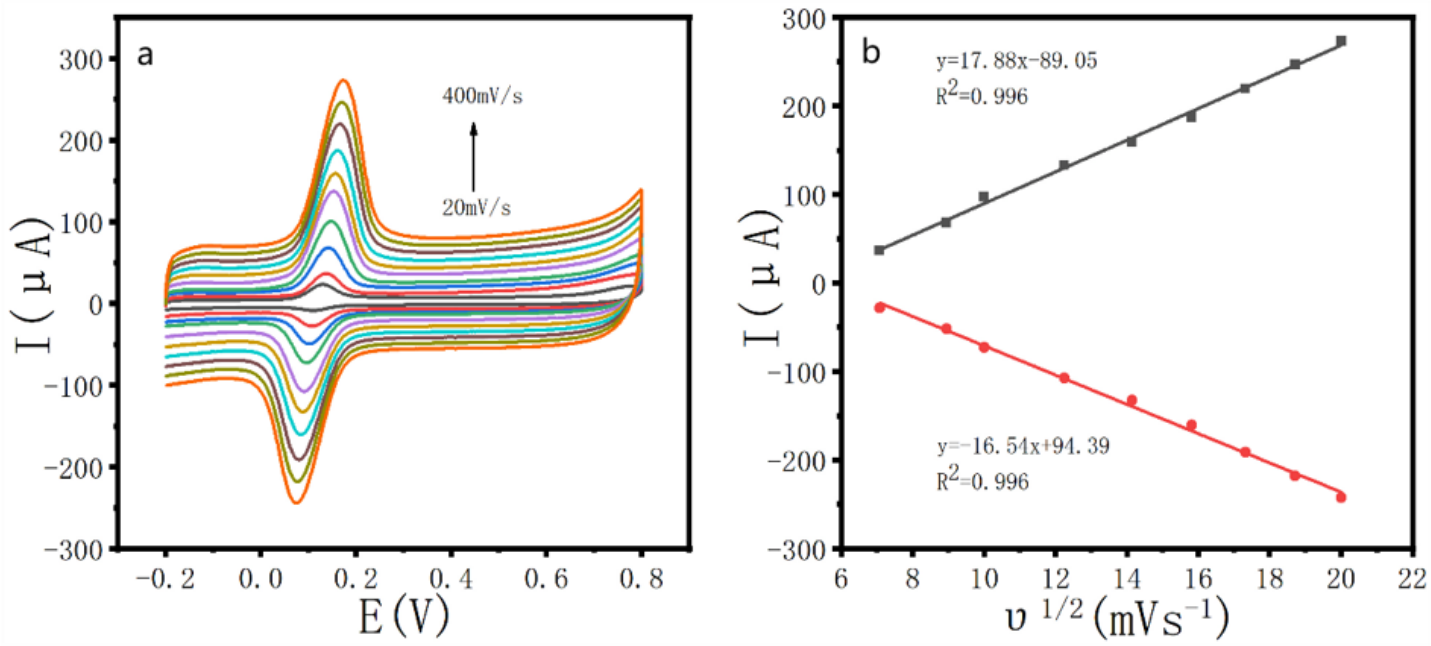

Figure 11

(a) CV of DA (100 μM) in phosphate buffer solution (pH 7.5) at different scan rates (20, 50, 80, 100, 150, 200, 250, 300, 350 and 400 mVs^{-1}), (b)Linear plot of peak current (Ip) versus square root of sweep speed ($\upsilon^{1/2}$).

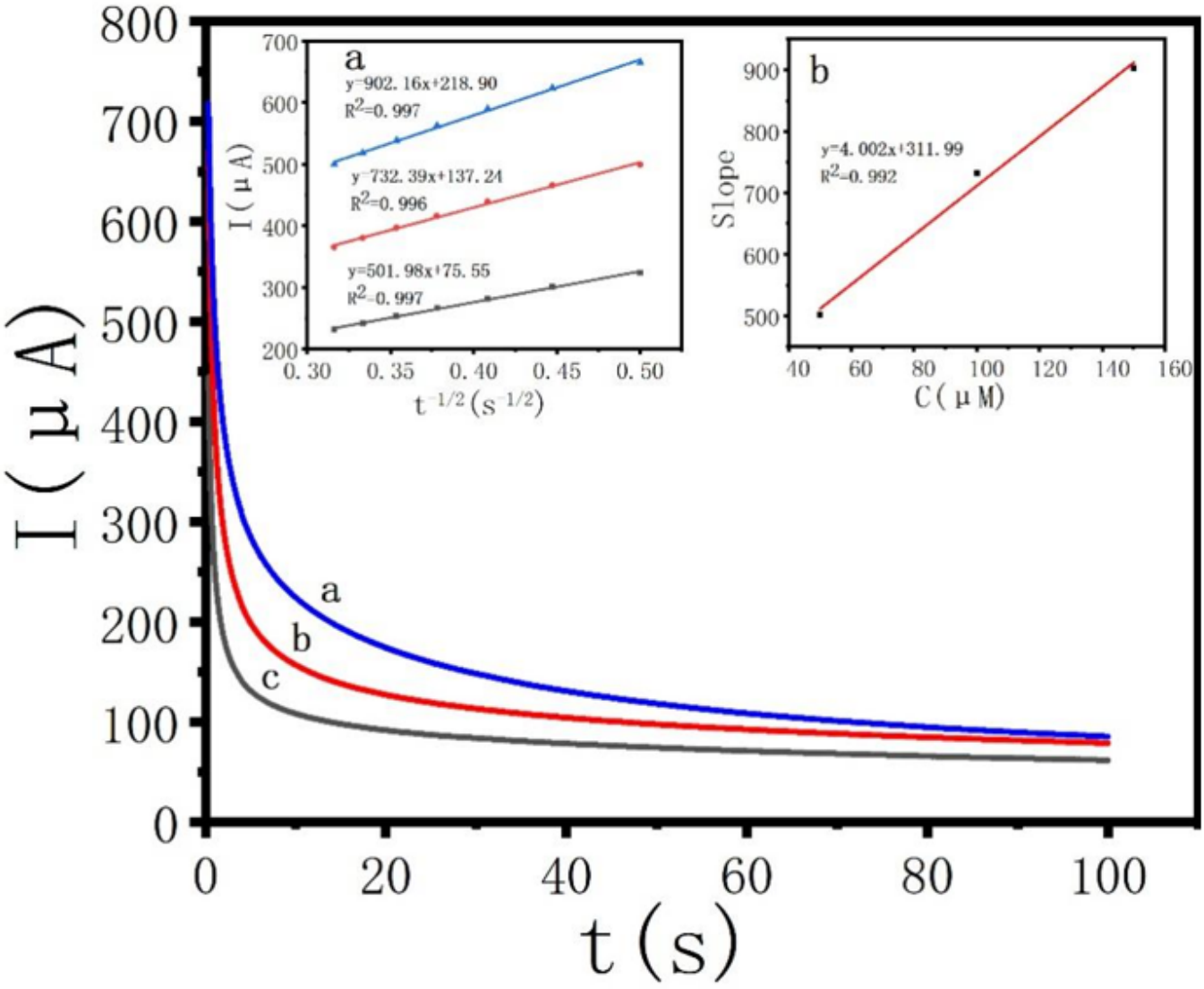

Figure 12

Chrono-current plots of C/PWA/GCE for different concentrations of DA (50, 100 and 150 μM) in phosphate buffer. Insets: (a) Plot of I versus $t^{-1/2}$ for different concentrations of DA (50, 100 and 150 μM) and (b) slope of the line obtained in inset a versus DA concentration.

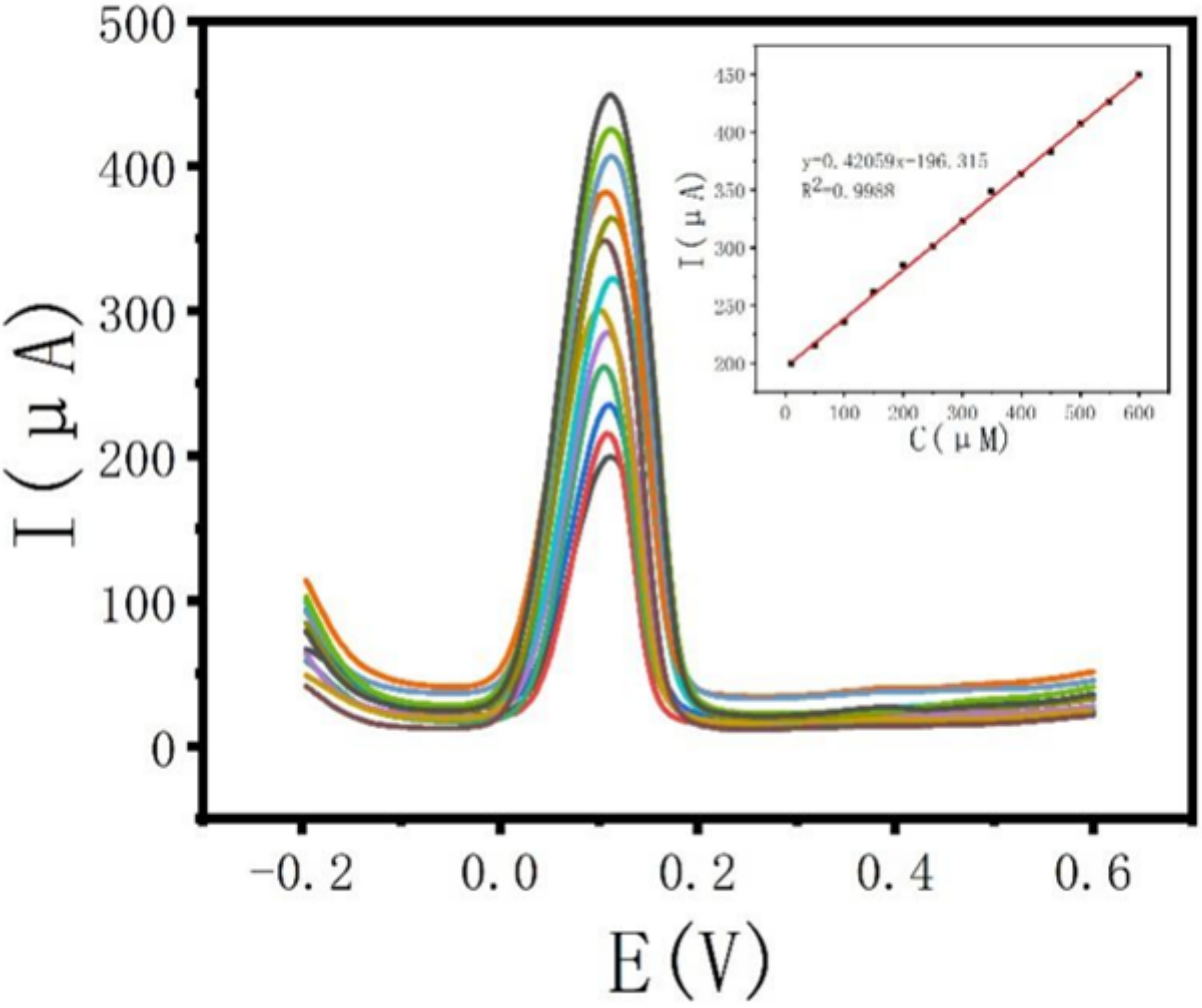

Figure 13

Differential pulse voltammograms for different concentrations of DA (10-600 μM) at C/PWA/GCE in phosphate buffer. Inset: Correlation calibration curves for a given concentration range.

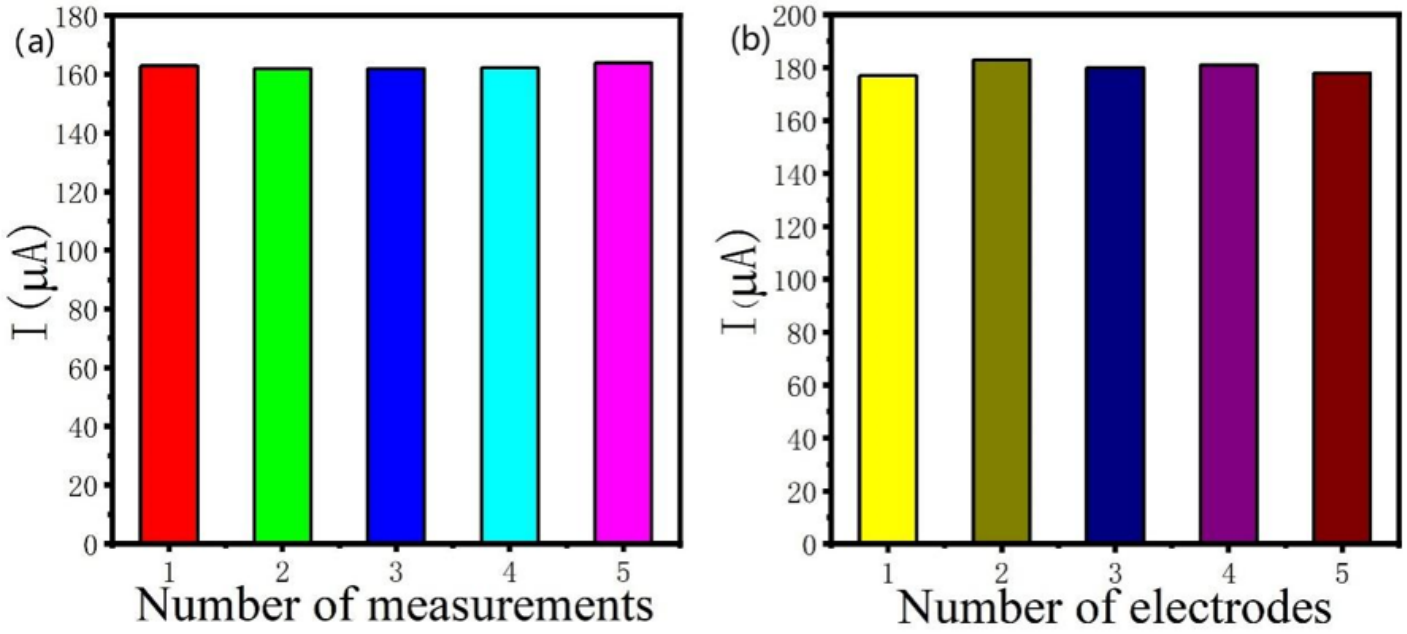

Figure 14

(a) Repeatability and (b) reproducibility measurements of the C/PWA/GCE sensor.